Applied Microbiology and Biotechnology (2024) 108:488
https://doi.org/10.1007/s00253-024-13325-w

MINI-REVIEW

L-rhamnose isomerase: a crucial enzyme for rhamnose catabolism and conversion of rare sugars

Hiromi Yoshida[1,2] · Ken Izumori[1,3] · Akihide Yoshihara[1,3]

Received: 28 August 2024 / Revised: 2 October 2024 / Accepted: 4 October 2024 / Published online: 16 October 2024

Abstract

L-rhamnose isomerase (L-RhI) plays a key role in the microbial L-rhamnose metabolism by catalyzing the reversible isomerization of L-rhamnose to L-rhamnulose. Additionally, the enzyme exhibits activity on various other aldoses and ketoses, and its broad substrate specificity has attracted attention for its potential application in the production of rare sugars; however, improvement of the enzyme properties is desirable, such as thermal stability, enzymatic activity, and a pH optimum suitable for industrial usage. This review summarizes our current insights into L-RhIs with respect to their substrate recognition mechanism and their relationship with D-xylose isomerase (D-XI) based on structural and phylogenetic analyses. These two enzymes are inherently different, but recognize distinctly different substrates, and share common features that may be phylogenetically related. For example, they both have a flexible loop region that is involved in shaping active sites, and this region may also be responsible for various enzymatic properties of L-RhIs, such as substrate specificity and thermal stability.

Key points

•*L-RhIs share structural features with D-XI.*
•*There are two types of L-RhIs: E. coli L-RhI-type and D-XI-type.*
•*Flexible loop regions are involved in the specific enzyme properties.*

Keywords D-xylose isomerase · *Lactobacillus rhamnosus* Probio-M9 · L-rhamnose isomerase · *Pseudomonas stutzeri* · Rare sugar

Introduction

Metabolism of L-rhamnose

L-rhamnose isomerase (E.C. 5.3.1.14)

L-rhamnose isomerase (L-RhI) is one of the inducible enzymes involved in the L-rhamnose metabolism in various microorganisms. L-rhamnose is a deoxy monosaccharide, and widely distributed in bacteria and plants (Jiang et al. 2021). L-RhI catalyzes the reversible isomerization between L-rhamnose and L-rhamnulose, which is the first step in the metabolism of L-rhamnose in the majority of bacteria including *Escherichia coli* (Wilson and Ajl 1957). Other enzymes participating in the breakdown of L-rhamnose are L-rhamnulose kinase, and L-rhamnulose-phosphate aldolase in *E. coli* (Takagi and Sawada 1964). The genes of these enzymes have been reported (Power 1967; Moralejo et al. 1993). As the first step of the catabolization in the cells, L-rhamnose (= 6-deoxy L-mannose) is converted to L-rhamnulose (= 6-deoxy L-fructose) by L-RhI, and this is followed by conversion to L-rhamnulose-1-phosphate (= 6-deoxy L-fructose-1-phosphate) by the above-mentioned kinase. L-rhamnulose 1-phosphate is further converted to dihydroxyacetone phosphate and L-lactaldehyde through the above-mentioned aldolase. Then, L-lactaldehyde is oxidized to L-lactate by L-lactaldehyde dehydrogenase and further converted to pyruvate by L-lactate dehydrogenase in aerobic

✉ Hiromi Yoshida
yoshida.hiromi@kagawa-u.ac.jp

1 International Institute of Rare Sugar Research and Education, Kagawa University, Kagawa, Japan

2 Department of Basic Life Science, Faculty of Medicine, Kagawa University, 1750-1 Ikenobe, Miki-Cho, Kita-Gun, Kagawa 761-0793, Japan

3 Faculty of Agriculture, Kagawa University, 2393 Ikenobe, Miki, Kagawa 761-0795, Japan

conditions, which is fed into the general metabolic pathways (Fig. 1a).

In general, *E. coli* cannot grow on L-lyxose as the sole carbon source. L-rhamnulose kinase does not phosphorylate L-xylulose sufficiently to support the growth of wild-type *E. coli*, but L-RhI can catalyze the conversion of L-lyxose to L-xylulose. The catabolic pathway of L-lyxose by using the L-rhamnose metabolism enzymes was found in mutant strains that grow on L-lyxose (Fig. 1a) (Badia et al. 1991).

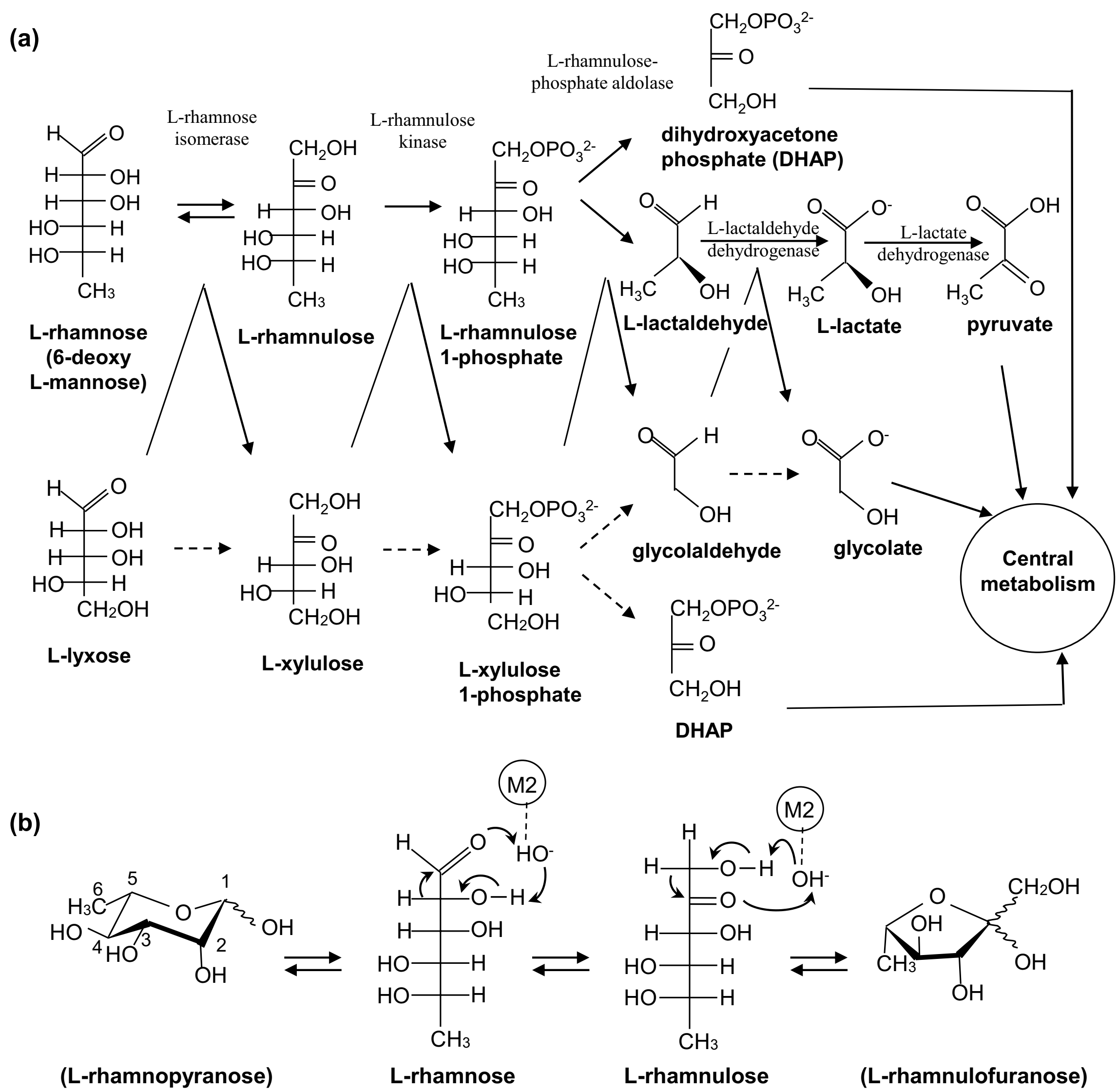

Fig. 1 The main catabolic pathway of L-rhamnose in *E. coli* and the proposed aldose-ketose isomerization catalyzed by L-RhIs based on the metal-mediated hydride-shift mechanism. **a** The catabolic pathway of L-RhI in *E. coli*. L-rhamnose (=6-deoxy L-mannose) is converted to L-rhamnulose (=6-deoxy L-fructose) by L-rhamnose isomerase (L-RhI), and this is followed by conversion to L-rhamnulose-1-phosphate (=6-deoxy L-fructose-1-phosphate) by L-rhamnulose kinase. The L-rhamnulose 1-phosphate is further converted to dihydroxyacetone phosphate and L-lactaldehyde through the catalysis of L-rhamnulose-phosphate aldolase. L-lactaldehyde is converted to L-lactate and pyruvate through the general metabolic enzymes of L-lactaldehyde dehydrogenase and L-lactate dehydrogenase, respectively (Badia et al. 1991). In general, wild-type *E. coli* cannot grow on L-lyxose as the sole carbon. L-rhamnulose kinase does not phosphorylate L-xylulose sufficiently, but L-RhI can catalyze the conversion of L-lyxose to L-xylulose. The indicated catabolic pathway of L-lyxose was found in mutant strains that grow on L-lyxose (Badia et al. 1991). **b** The chemical reaction between L-rhamnose and L-rhamnulose with sugar-ring form, catalyzed by L-RhIs from *E. coli* (Korndörfer et al. 2000) and *P. stutzeri* (Yoshida et al. 2007, 2010b, 2012). M2 represents the catalytic metal ion

Catalytic mechanism of L-RhIs

The proposed catalytic reaction of L-RhIs for aldose-ketose isomerization uses a metal-mediated hydride-shift mechanism. The X-ray structures of L-RhIs show a homotetramer, and each subunit contains an active site with two metal ions (a structural metal (M1) and a catalytic metal (M2) ion). In Fig. 1b, only the catalytic metal is presented. Here, a proton is transferred between O1 and O2 of the substrate by a catalytic water molecule, which binds to the catalytic metal ion to be activated as a hydroxide ion (Fenn et al. 2004; Kovalevsky et al. 2008). A catalytic reaction mechanism catalyzed by L-RhIs was proposed for *E. coli* (Korndörfer et al. 2000) and for *Pseudomonas stutzeri* (Yoshida et al. 2007, 2010b, 2012). M2 represents a catalytic metal ion and activates the catalytic water.

This review presents recent studies of L-RhIs based on structural analysis, since the enzyme properties of various L-RhIs for rare sugar production have been reported and discussed in a recent review article (Mahmood et al. 2024). We discuss the flexible region that is involved in the active site and responsible for various enzymatic properties of L-RhIs.

L-RhIs from various microorganisms

Before the 1990s, L-RhIs from a few bacteria, *Pasteurella pestis* (Englesberg. 1957), *Salmonella typhimurium* (Englesberg and Baron 1959; Akhy et al. 1984; Al-Zarban et al. 1984), *Lactobacillus plantarum* (Domagk and Zech 1963), and *Arthrobacter pyridinolis* (Levinson and Krulwich 1976) have been reported to be involved in the metabolism of L-rhamnose. In 1997, a novel L-RhI from a mutant *Pseudomonas* sp. strain LL172 was reported to harbor broad substrate specificity (Bhuiyan et al. 1997). The enzyme showed activity not only toward L-rhamnose, but also L-lyxose, L-mannose, D-gulose, D-ribose, D-allose, and L-talose. In *E. coli* mutant cells that can grow on L-lyxose, L-lyxose has been reported to be metabolized via the L-rhamnose pathway, and L-lyxose was converted to L-xylulose by L-RhI (Fig. 1a, Badia et al. 1991). L-RhI from *E. coli* (EcL-RhI) showed activity toward L-rhamnose and L-lyxose. Later, L-RhI from *Pseudomonas stutzeri* (PsL-RhI) was further characterized, and the enzyme was found to catalyze the reversible isomerization between D-allulose and D-allose (Leang et al. 2004a, b). Currently, D-allulose and D-allose are known as rare sugars that exhibit physiological functions. D-Allulose exhibits suppression of postprandial blood-sugar elevation and the accumulation of visceral fat (Hayashi et al. 2010; Iida et al. 2013). D-Allose exhibits anti-oxidation and anti-tumor effects (Sun et al. 2006; Nakamura et al. 2011; Noguchi et al. 2016; Shintani et al. 2020). These rare sugars are beneficial products and demand for them is increasing in the food and pharmaceutical industries. For enzymatic production of rare sugars, a variety of ketose epimerases, aldose-ketose isomerases and oxidoreductases are applied using abundant sugars such as D-fructose, based on the Izumoring strategy (Izumori 2002, 2006; Granström et al. 2004). D-fructose is converted to D-allulose by ketose 3-epimerase, and the resulting D-allulose is further converted to D-allose by L-RhI, which can catalyze the isomerization between D-allulose and D-allose. As such, L-RhI is a promising enzyme for D-allose production, and numerous L-RhIs have been reported for this purpose: L-RhIs form *Bacillus pallidus* (Poonperm et al. 2007), *Thermoanaerobacterium saccharolyticum* (TsL-RhI; Lin et al. 2010), *Thermotoga maritima* (Park et al. 2010), *Caldicellulosiruptor saccharolyticus* (CasL-RhI; Lin et al. 2011), *Bacillus halodurans* (BhL-RhI; Prabhu et al. 2011), *Mesorhizobium loti* (Takata et al. 2011), *Dictyoglomus turgidum* (Kim et al. 2013), *Bacillus subtilis* (BsL-RhI; Park 2014; Bai et al. 2015), *Thermobacillus composti* (Xu et al. 2017), *Clostridium stercorarium* (ClsL-RhI; Seo et al. 2018), *Caldicellulosiruptor obsidiansis* (CaoL-RhI; Chen et al. 2018a, b), and *Shinella zoogloeoides* (Morimoto et al. 2022). In a recent study, recombinant L-RhIs based on genome analysis were characterized: L-RhI from the probiotic bacterium *Lactobacillus rhamnosus* Probio-M9 (LrL-RhI; Yoshida et al. 2024) and L-RhI from hot spring metagenome DNA that was phylogenetically close to *Chloroflexus islandicus* (Sharma et al. 2024). These L-RhIs show broad substrate specificity and have the potential to produce various rare sugars. However, the enzyme activity of L-RhIs on D-allose is not sufficient for industrial usage, and studies on protein engineering of some L-RhIs to improve their enzymatic properties have been reported (Chen et al. 2018a, b; Tseng et al. 2022; Duan et al. 2023; Wei et al. 2023).

Table 1 gives pertinent details on various L-RhIs, among which catalytic activity, molecular mass, oligomeric state, etc. The first reported enzymatic properties of the native enzyme derived from native strains were further clarified through analyses of recombinant enzymes. Information on the enzymatic properties of EcL-RhI are summarized (Takagi and Sawada 1964; Badia et al. 1991; Korndörfer et al. 2000; Poonperm et al. 2007). Though EcL-RhI exhibits enzyme activity toward L-rhamnose, L-lyxose, and L-mannose, it does not seem to exhibit wide substrate specificity compared to other L-RhIs (Poonperm et al. 2007). PsL-RhI was the first reported enzyme to catalyze the reversible isomerization between D-allulose and D-allose. The reported kinetic parameters of recombinant PsL-RhI in each study

Table 1 Comparison of the enzyme properties of various L-RhIs

Source of enzyme	Native/subunit molecular mass (kDa)	Sequence information from the available database (NCBI)	Opt. pH	Opt. temp. (℃)	Metal ion	Km (mM)	kcat/Km (S^{-1} mM^{-1})	Vmax ($U{\bullet}mg^{-1}$)	Other substrates	Reference
Bacillus halodurans ATCC BAA-125	121/48, homodimer homotetramer*	*Halalkalibacterium halodurans* ATCC BAA-125 (BAB05271.1), 418 a.a., 48,178 Da	7.0	70	Mn^{2+}	528	0.28	187	L-lyxose >, L-mannose, D-gulose, L-talose	Prabhu et al. 2011 Prabhu et al. 2014*
Bacillus pallidus Y25	NR/48	*Aeribacillus pallidus* Y25 (BAF80456.1), 412 a.a., 47,637 Da	7.0	65	Mn^{2+} or Co^{2+}	4.89	13.9	87.0 (77.2)	L-mannose, L-lyxose, D-allose, D-ribose	Poonperm et al. 2007
Bacillus subtilis ATCC23857	194/49, homotetramer	*Bacillus subtilis* BSn5 (YP_004204944), 424 a.a., 48,603 Da	8.0	60	Mn^{2+}	53	2.89	3.58	L-lyxose, L-mannose, D-allose, D-gulose, D-ribose, L-talose	Park et al. 2014
Bacillus subtilis str. 168	NR/48	*Bacillus subtilis* strain 168 (CAB15096.1), 424 a.a., 48,645 Da	8.5	70	Mn^{2+}	0.49	15.8	1.54	D-ribose, L-mannose, D-allose	Bai et al. 2015
Caldicellulosiruptor obsidiansis OB47	112/48, homodimer	*Caldicellulosiruptor obsidiansis* strain OB47 (ADL41970.1), 426 a.a, 48,390 Da	8.0	85	Co^{2+}	3.54	56.4	277.6	L-mannose, D-allose, L-fructose	Chen et al. 2018a J.Sci.Food Agric
Caldicellulosiruptor saccharolyticus ATCC 43494	193/48, homotetramer	*Caldicellulosiruptor saccharolyticus* ATCC 43494 (ABP66492.1), 426 a.a., 48,294 Da	7.0	90	Co^{2+}	1.03	97.1	380	L-lyxose, L-mannose, D-allose, D-ribose	Lin et al. 2011
Chloroflexus islandicus	190/47	*Chloroflexus islandicus*, (OAN47027.1), 426 a.a., 46,873 Da	7.0	75	Mn^{2+}	110	2.98	N.R	D-allulose, D-galactose, D-allose, D-glucose, D-ribose	Sharma et al. 2024
Clostridium stercorarium ATCC 35414	154/49, homotrimer	*Thermoclostridium stercorarium* strain ATCC 35414 (AGC67668.1), 425 a.a., 48,175 Da	7.0	75	Mn^{2+}	1.36	148.9	520	L-lyxose, L-mannose, D-allose, L-fructose, D-ribose	Seo et al. 2018
Dictyoglomus turgidum DSMZ6724	185/46, tetramer	*Dictyoglomus turgidum* strain DSM 6724 (ACK41729.1), 397a.a., 45,873 Da	8.0	75	Mn^{2+}	24.6	7.93	N.R	L-lyxose, L-mannose, L-xylulose, L-fructose, D-allose, D-ribose	Kim et al. 2013

Table 1 (continued)

Source of enzyme	Native/subunit molecular mass (kDa)	Sequence information from the available database (NCBI)	Opt. pH	Opt. temp. (℃)	Metal ion	Km (mM)	kcat/Km (S^{-1} mM^{-1})	Vmax (U•mg^{-1})	Other substrates	Reference
Escherichia coli	NR/47		7.6	60[⁑]	Mn^{2+}	2.0	NR	6.2 65.8[⁑]	L-lyxose, L-mannose[⁑]	Takagi & Sawada. 1964 Badia et al. 1991 Poonperm et al. 2007[⁑]
Escherichia coli	188/47 homotetramer	*Escherichia coli* strain K12 (CAA43002.1), 419 a.a., 47,199 Da	7.6	NR	Mn^{2+}	NR	NR	NR		Korndörfer et al. 2000
Lactobacillus rhamnosus Probio M9	NR/49, homotetramer	*Lacticaseibacillus rhamnosus* (WP_019728362.1), 426 a,a,, 48,707 Da	5.5	70	Co^{2+}	NR	NR	173.1	L-lyxose, L-mannose, D-ribose, D-allose	Yoshida et al. 2024
Mesorhizobium loti Tono	NR/47	*Rhizobium loti* TONO (BAK52808.1), 430 a.a., 46,939 Da	9.0	60	Mn^{2+}	5	10.1	64.5	L-lyxose, D-ribose, L-talose, D-allose, L-mannose	Takata et al. 2011
Pseudomonas stutzeri	NR/43 NR/47[∫], homotetramer[∫]	*Stutzerimonas stutzeri* (BAD14073.1), 430 a.a., 46,975 Da	9.0	60	Mn^{2+}	11 11.9[⁑]19.4[∬]	15.6 (as 43 kDa) 14.4[⁑] 11.6[∬]	240 244[⁑] 280[∬]	L-mannose, L-lyxose, D-ribose, D-allose, D-xylose	Leang et al. 2004a,b Yoshida et al. 2007[∫] Poonperm et al. 2007[⁑] Yoshida et al. 2010a[∬]
Pseudomonas sp. strain LL172	NR/42		9.0	60	Mn^{2+}	55	NR	182.6	L-lyxose, L-mannose, D-ribose, D-gulose, D-allose, L-talose	Bhuiyan et al. 1997
Shinella zoogloeoides NN6	162/43, homotetramer	Not available. As a reference, *Shinella zoogloeoides* (*Crabtreella saccharophila*), (MXO00413.1) 430 a.a., 46,819 Da	9.0	60	Mn^{2+}	18.5	50.7	NR	D-allose	Morimoto et al. 2022
Thermoanaerobacterium saccharolyticum NTOU1	NR/49	*Thermoanaerobacterium saccharolyticum*, NTOU1 (ADF43732.1), 425 a.a., 48,961 Da	7.0	75	Co^{2+}	3.53	50.8	203	L-lyxose, L-mannose, D-allose, D-ribose	Lin et al. 2010

Table 1 (continued)

Source of enzyme	Native/subunit molecular mass (kDa)	Sequence information from the available database (NCBI)	Opt. pH	Opt. temp. (℃)	Metal ion	Km (mM)	kcat/Km (S^{-1} mM^{-1})	Vmax (U•mg^{-1})	Other substrates	Reference
Thermobacillus composti KWC4	190/45, tetramer	*Thermobacillus composti* KWC4 (AGA57429.1), 420 a,a., 46,850 Da	7.5	65	Mn^{2+}	33.8	0.587	83	L-mannose, D-allulose, D-allose	Xu et al. 2017
Thermotoga maritima ATCC43589	184/46, homotetramer	*Thermotoga maritima* strain ATCC 43589 (AAD36148.1), 383 a.a., 44,732 Da	8.0	85	Mn^{2+}	37	3.95	55	L-lyxose, L-mannose, D-allose, D-gulose, D-ribose	Park et al. 2010

were similar, but they have been updated based on the estimated molecular mass. K_m, k_{cat}/K_m, and V_{max} with L-rhamnose as substrate are 11–19.4 mM, 11.6–15.6 s^{-1} mM^{-1}, and 240–280 U/mg (Leang et al. 2004a, b; Poonperm et al. 2007; Yoshida et al. 2010a). It is possible to estimate the molecular mass of other recombinant L-RhIs based on their sequences. In Table 1, the number of amino acid residues of L-RhIs is between 383 and 430, and the molecular mass of the subunit of L-RhIs is estimated to be between 45 and 49 kDa based on the available sequences from the database (NCBI). BhL-RhI was first reported as a homodimer after gel filtration analysis (Prabhu et al. 2011), but later updated to form a homotetramer in X-ray structure analysis (Prabhu et al. 2014). Although a few L-RhIs have been estimated to be dimer (BhL-RhI, Prabhu et al. 2011; CaoL-RhI, Chen et al. 2018a) and trimer (ClsL-RhI, Seo et al. 2018) in a solution following gel filtration chromatography analysis, L-RhIs generally form homotetramers as a stable form based on the structural analysis of other L-RhIs (described later).

The optimal pH of L-RhIs has been from neutral to basic before the characterization of LrL-RhI was reported (Yoshida et al. 2024). Recombinant LrL-RhI is derived from the probiotic lactic acid bacterium *L. rhamnosus* Probio-M9 that was isolated from human colostrum (Liu et al. 2020; Ruibo et al. 2023). As was expected from the cell growth condition, the optimal pH of LrL-RhI is pH 5.5. Since a basic condition could cause non-enzymatic aldose-ketose isomerization, yielding a coproduct, pH-shift engineering of L-RhI would likely improve the target enzyme properties.

As for the optimal temperature, it has been reported to be between 60 and 90 ℃. The highest optimal temperature was reported for CasL-RhI, which also exhibits high catalytic activity (kcat/Km 97.1 s^{-1} mM^{-1}). The highest enzyme activity detected so far is 148.9 s^{-1} mM^{-1} of CsL-RhI.

Crystal structures and flexible loop region

Overall structures and its relationship with that of D-XI

The crystal structure of EcL-RhI (PDBID: 1D8W) was the first determined structure (Korndörfer et al. 2000), and this was followed by the structure of PsL-RhI (2HCV, Yoshida et al. 2007), BhL-RhI (3UU0, Prabhu et al. 2014), and LrL-RhI (8JQ3, Yoshida et al. 2024). These L-RhIs form homotetramers (Fig. 2a–d), and each subunit adopts a $(\beta/\alpha)_8$- barrel fold (Fig. 3a–d). The structure of EcL-RhI in complex with L-rhamnose (EcL-RhI/L-rhamnose, 1DE6, Fig. 3a) is comparable to the subunit structure of D-XI from *Streptomyces rubiginosus* in complex with D-xylose (SrD-XI/D-xylose, 4XIS, Whitlow et al. 1991, Fig. 3e), as they share a common $(\beta/\alpha)_8$-barrel fold and

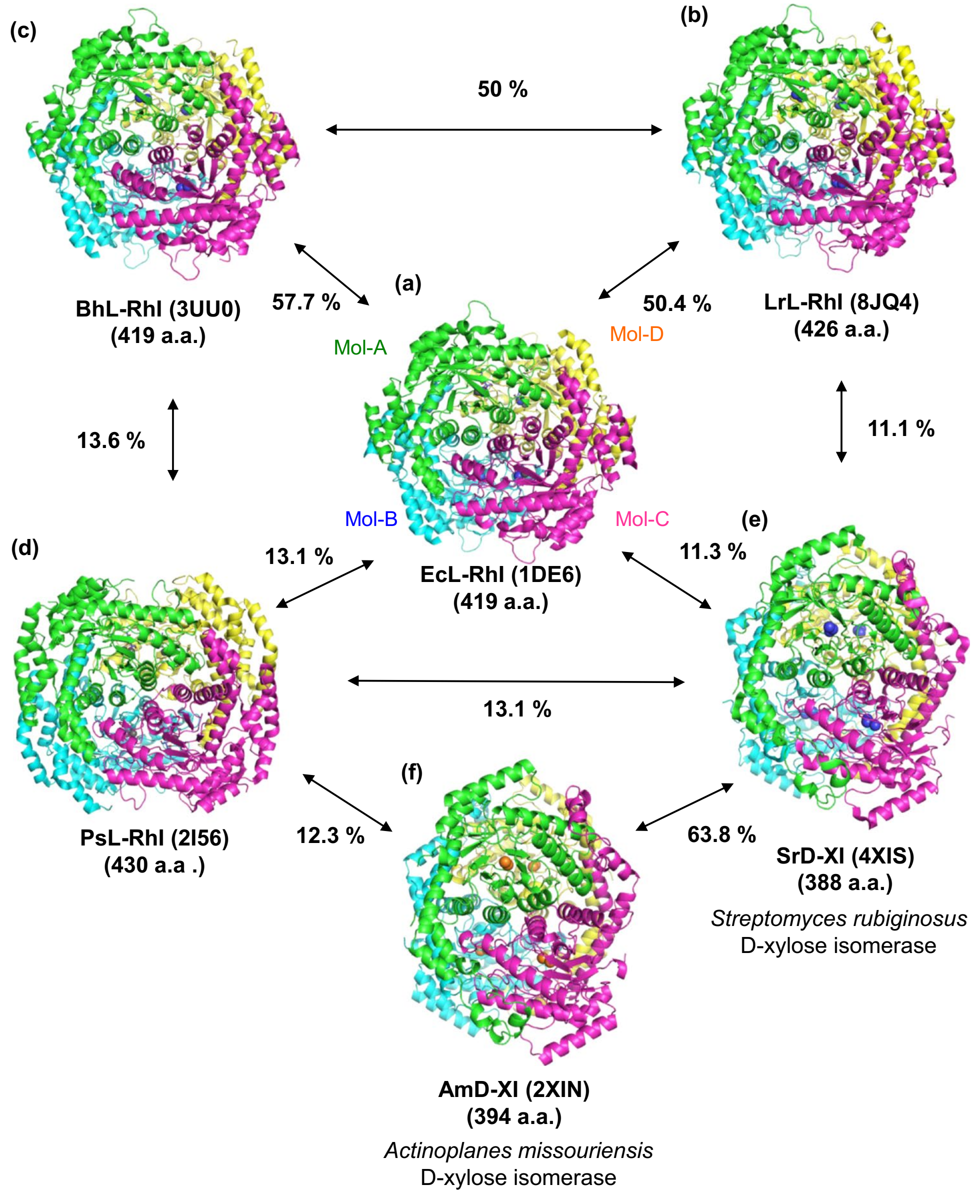

Fig. 2 Overall structures of L-RhIs and D-XIs. Overall structures of homotetrameric **a** EcL-RhI (labeled with Mol-A, Mol-B, Mol-C, and Mol-D), **b** LrL-RhI, **c** BhL-RhI, **d** PsL-RhI, **e** D-XI from *Streptomyces rubiginosus* (SrD-XI), and D-XI from *Actinoplanes missouriensis* (AmD-XI). Metal ions (structural and catalytic metals) are shown as spheres. The values with arrows indicate the sequence identities between the enzymes

similar metal binding in the active site (metal ions are required for enzyme activity). The homotetrameric form of L-RhIs has almost the same appearance except for a slightly different PsL-RhI due to a longer sequence (430 a.a.) (Fig. 2a–d). Although EcL-RhI and SrD-XI share a common fold in the monomeric structure (Fig. 3a, 3e), the tetrameric arrangement of SrD-XI (Fig. 2e) differs from that of other L-RhIs. (Fig. 2a–d). The homotetrameric structure of SrD-XI is similar to that of D-XI from *Actinoplanes missouriensis* (AmD-XI, 2XIN, Jenkins et al. 1992, Fig. 2f). D-XIs also form homotetramers, and their structures are similar among the family of D-XIs. In Fig. 3, subunit structures and dimeric forms of L-RhIs and SrD-XI are compared. At the center of each barrel, the catalytic site with two metal ions (shown as spheres) is located with part of a flexible loop region (β1–α1 loop colored in red). Since the red-colored loop regions are highly mobile, part of the β1–α1 loop regions are missing or their occupancies are low in the crystal structures of EcL-RhI, BhL-RhI, and LrL-RhI. The regions show a high plasticity in the structure of L-RhIs without bound substrates. The loop region becomes stabilized when substrate is bound. The structure of LrL-RhI in complex with D-allulose (LrL-RhI/D-allulose, 8JQ5) showed the whole β1–α1 loop region in Mol-A, but this was missing in Mol-D (Fig. 3b, right side in dimeric unit). The flexible loop may be stabilized depending on the substrate and involved in catalytic efficiency. The flexible loop of PsL-RhI in complex with L-rhamnose (PsL-RhI/L-rhamnose, 2I56) covers the active sites of the neighboring subunit at the dimer

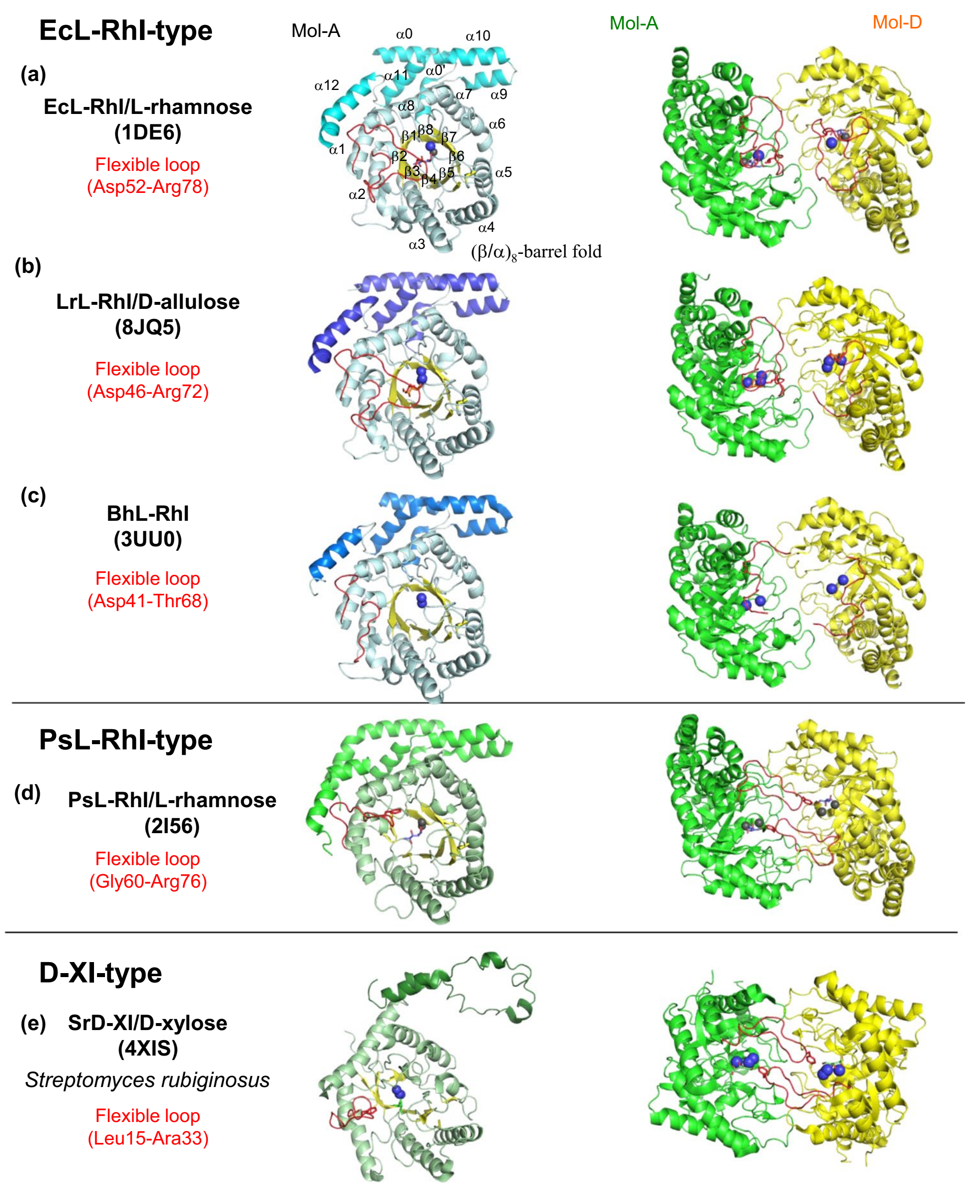

Fig. 3 Overall structures of monomer and dimeric units of L-RhIs and SrD-XI. Overall structures of monomeric (Mol-A) and homodimeric (Mol-A and Mol-D): **a** EcL-RhI/L-rhamnose, **b** LrL-RhI/D-allulose, **c** BhL-RhI, PsL-RhI/L-rhamnose, **d** PsL-RhI/L-rhamnose, and **e** SrD-XI/D-xylose. The highly flexible loop (β1-α1 loop) regions are colored in red. The bound substrate and metal ions are shown as sticks and spheres, respectively. Part of the flexible loop regions is missing in LrL-RhI (Mol-A) and BhL-RhI (Mol-A and Mol-D)

interface (Fig. 3d, dimeric unit). This swapping mode for covering the active site is responsible for the active site of the neighboring subunit, indicating that the dimeric unit is important for creating the catalytic site as found in SrD-XI (Fig. 3e, dimeric unit), while in EcL-RhI, the corresponding flexible loop covers the active site of the self-subunit to form the catalytic site in the subunit (Fig. 3a). BhL-RhI and LrL-RhI contain a similar active site with a loop from their own subunit (EcL-RhI type) that is different from the PsL-RhI type and D-XI type. The active site formation of PsL-RhI is unique and has not been reported for the structure of other L-RhIs; however, various L-RhIs have been reported, and they might be categorized as EcL-RhI-type or PsL-RhI-type (similar to D-XI-type). In addition, the flexible loop may be also involved in the observed different oligomer states of L-RhIs in solution. Table 2 summarizes the comparison of sequence identities and the formation of the active site in L-RhIs and D-XIs. PsL-RhI is likely in between the EcL-RhI-type and D-XI-type.

The structure of the active site and its relationship with that of D-XI

The structures of the substrate-binding sites of EcL-RhI/L-rhamnose, PsL-RhI/L-rhamnose, LrL-RhI/D-allulose, and SrD-XI/D-xylose are shown in Fig. 4a–d. In EcL-RhI (Fig. 4a), hydrophobic residues (Val53, Leu63, and Ile67) from the flexible loop create a hydrophobic pocket to stabilize substrate binding. The corresponding hydrophobic residues in LrL-RhI (Fig. 4c) are Ile47, Leu57, and Ile61. In PsL-RhI (Fig. 4b), there is no corresponding hydrophobic

Table 2 Comparison of L-RhIs and D-XI with the values of sequence identities based on the sequence database and formation of active site

Enzyme (Number of the residues)	EcL-RhI	BhL-RhI	LrL-RhI	PsL-RhI	SrD-XI	AmD-XI	Formation of active site
EcL-RhI (419 a.a.)	100 %	57.7 %	50.4 %	13.1 %	11.3 %	10.9 %	self-subunit
BhL-RhI (419 a.a.)	57.7 %	100 %	50 %	13.6%	11.3 %	12.4 %	self-subunit
LrL-RhI (426 a.a.)	50.4 %	50 %	100 %	12.2 %	11.1 %	10.9 %	self-subunit
PsL-RhI (430 a.a.)	13.1 %	13.6%	12.2 %	100 %	13.1 %	12.3 %	with neighboring subunit
SrD-XI (388 a.a.)	11.3 %	11.3 %	11.1 %	13.1 %	100 %	63.8 %	with neighboring subunit
AmD-XI (394 a.a.)	10.9 %	12.4 %	10.9 %	12.3 %	63.8 %	100 %	with neighboring subunit

A group belonging to E. coli L-RhI type was colored with cyan, and another group belonging to D-XI is colored with light green. PsL-RhI colored with pink is located on the border between the groups

pocket, and *Phe66 from a neighboring subunit causes hydrophobic interactions with the substrate. SrD-XI similarly creates hydrophobic interactions by *Phe26 from a neighboring subunit.

L-RhIs and D-XIs require two metal ions for their activity. They are metal dependent enzymes and have metal ion selectivity to exhibit the highest activity. Various metal ion species could bind at two metal binding sites for a structural metal (M1) and a catalytic metal (M2). The "structural metal" is to stabilize the substrate binding, and the "catalytic metal" is to promote the hydride shift as described in Fig. 1b. Most of L-RhIs show the highest activity in the presence of Mn^{2+} or Co^{2+} (Mahmood et al. 2024). As shown in Table 1, Mn^{2+} is preferable metal ion in EcL-RhI and PsL-RhI. In addition, structural and catalytic metal ions are removable by EDTA treatment and could be replaced with another metal ion in the excess of any metal ion. Since the catalytic metal ion is mobile between two positions as found in our previous study on PsL-RhI (Yoshida et al. 2010b) and also known in D-XIs (Jenkins et al. 1992; Lavie et al. 1994; Hagedoorn et al. 2024), dissociation constant of catalytic metal ion would be different from that of structural metal ion. In some crystal structures of L-RhIs and D-XIs, different metal ion species bind at catalytic and structural metal ion binding sites.

In Fig. 4a (EcL-RhI/L-rhamnose, 1DE6), structural metal ion (M1, gray for Zn^{2+}) and catalytic metal ion (M2, blue for Mn^{2+}) are shown as spheres. Water molecules are shown as red spheres in Figs. 4b, 4c, and 4d. In PsL-RhI/L-rhamnose (2I56, Fig. 4b), the metal ions (M1 and M2 are Zn^{2+}, lower activity) are coordinated in a distorted octahedral form with six coordination bonds. M1 coordinates with *Glu219*, *Asp254*, *His281*, *Asp327*, O2, and O3 of the substrate (L-rhamnose). M2 coordinates with *His257*, *Asp289*, O1, and O2 of the substrates, catalytic water (labeled as W), and other water molecules. These residues (labeled with underlines) coordinating metal ions are conserved in L-RhIs (Figs. 4a, 4b, 4c), and most of them are also conserved in SrD-XI (M1 and M2 are Mn^{2+}, Fig. 4d) except for Glu217 and Asp245 which correspond to Asp254 and His281 of PsL-RhI, respectively. Since M1 of SrD-XI interacts with Glu181, Glu217, Asp245, Asp287, O2, and O4 of the substrate (D-xylose), these residues for metal binding sites are conserved in D-XIs. In L-RhIs, O1, O2, and O3 of the substrate coordinate with metal ions, and configurations of C2 and C3 of the substrate are important for substrate recognition and enzyme activity. The configurations of C2 and C3 of L-rhamnose, L-lyxose, D-allulose, and D-allose are the same. In D-XIs, O1, O2, and O4 of the substrate coordinate with metal ions; thus, the configuration of C2 and C4 of the substrate are important for substrate recognition. Substrate recognition is inherently different between L-RhIs and D-XIs.

In the case of favorable metal ion (Mn^{2+}) bound in M1 and M2 of the active site, the catalytic metal is mobile between the two positions (M2A and M2B) as shown with the arrows (Fig. 4c, 4d). As this metal movement

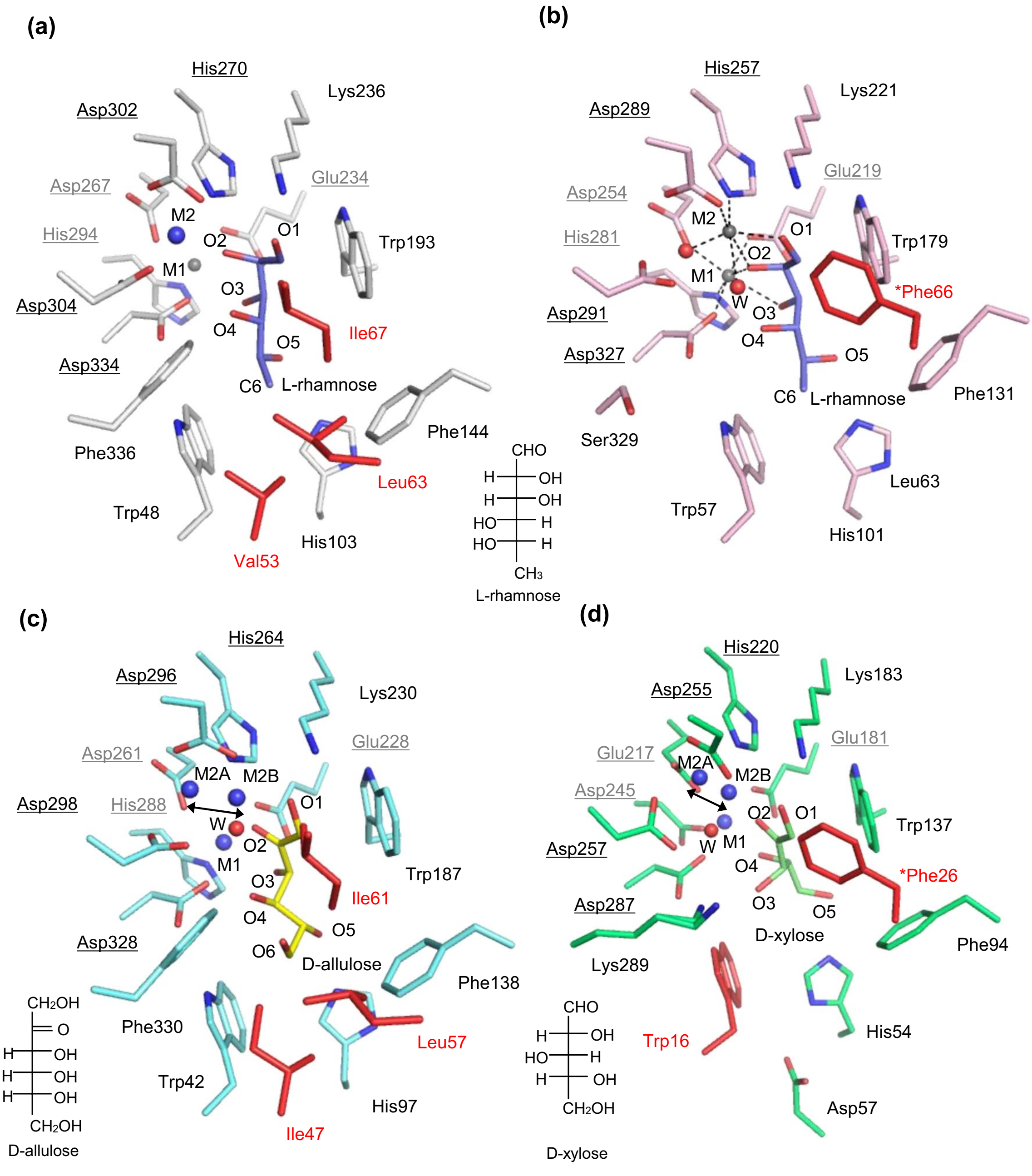

Fig. 4 Substrate-binding site of L-RhIs and D-XI. **a** EcL-RhI/L-rhamnose, **b** PsL-RhI/L-rhamnose, **c** LrL-RhI/D-allulose, and **d** SrD-XI/D-xylose. The metal ions are shown as spheres (blue for Mn^{2+}; gray for Zn^{2+}) labeled with M1 (structural metal) and M2 (catalytic metal) in EcL-RhI. Observed catalytic waters are shown as red spheres in PsL-RhI, LrL-RhI, and SrD-XI. In the case of Mn^{2+} (both M1 and M2 are Mn^{2+} in LrL-RhI and SrD-XI), the catalytic metal is mobile between the two positions (M2A and M2B) as shown with the arrows. As this metal movement is observed in the presence of favorable metal ions that exhibit high catalytic activity, the metal movement could be involved in the catalytic efficiency of L-RhIs. In PsL-RhI of the Mn^{2+}-bound structure without a substrate, M2 was found at the positions of M2A or M2B in each subunit (Yoshida et al. 2010a, b). The bound L-rhamnose (purple stick), D-allulose (yellow stick), and D-xylose (light green stick) are shown in the active site with labels. The amino acid residues in the flexible loop regions are colored in red. *Phe indicates the residue from the neighboring subunit

is observed in the presence of favorable metal ions that exhibit high catalytic activity in PsL-RhI (Yoshida et al. 2010b), the metal movement could be involved in the catalytic efficiency of L-RhIs. In PsL-RhI of the Mn^{2+}-bound structure without a substrate, M2 was found at the positions of M2A or M2B in each subunit (Yoshida et al. 2010b). As shown in L-RhIs and D-XI, the backward of the catalytic reaction with metal ions is shielded by Trp

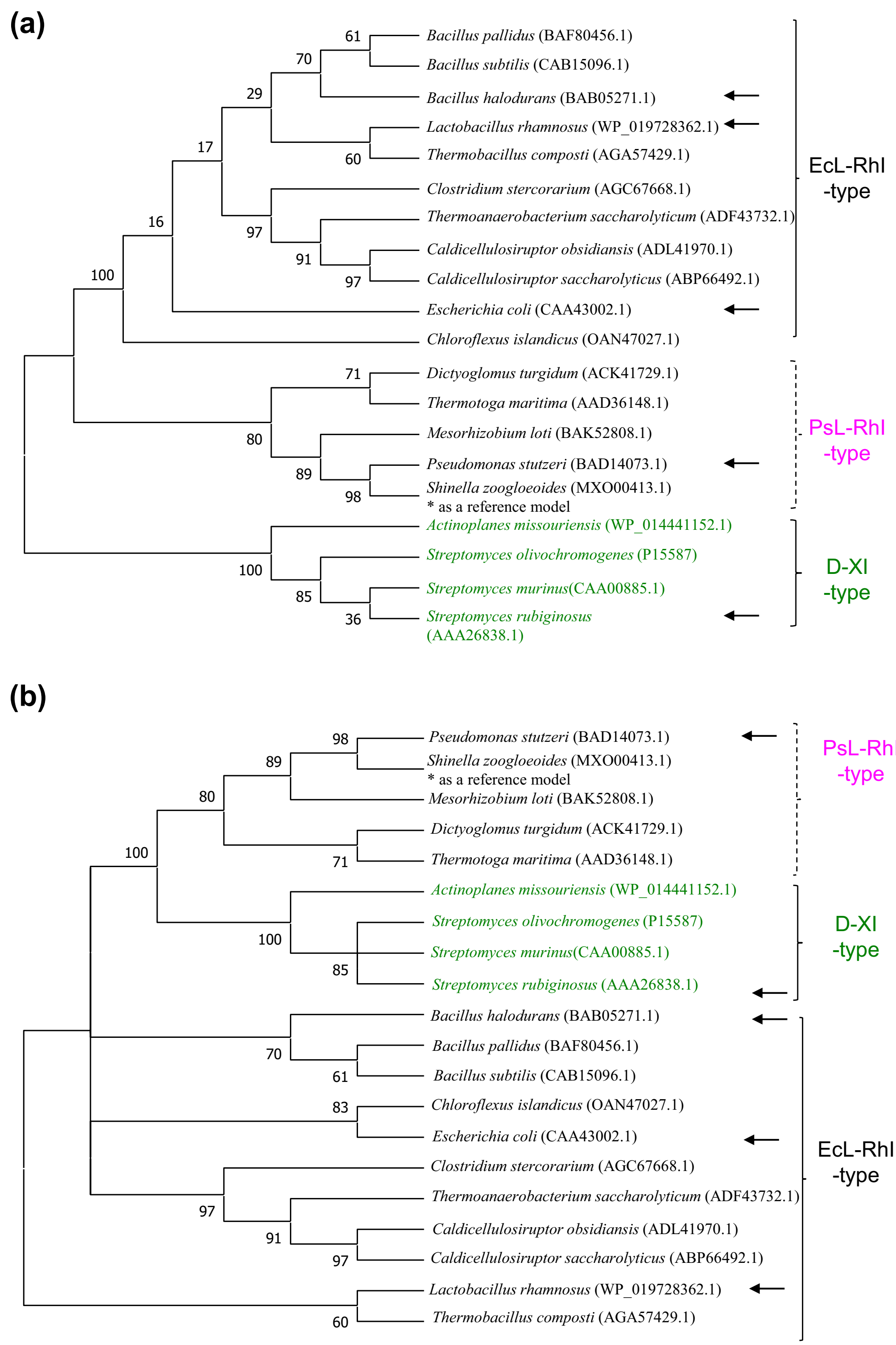

Fig. 5 Phylogenetic analysis of L-RhIs and D-XIs. **a** Initial tree for the heuristic search and **b** the obtained phylogenetic tree after evolutionary analysis. The phylogenetic trees were constructed by MEGA11 (Tamura et al. 2021) using the Maximum Likelihood method. The source with accession numbers of L-RhIs and D-XIs are shown in black and green letters, respectively. The arrows indicate the source of the structures which are available and compared in this review. A predicted group as PsL-RhI type is presented with a dashed line and pink label. The initial tree for the heuristic search was obtained automatically by applying Neighbor-Join and BioNJ algorithms to a matrix of pairwise distances estimated using the JTT model and then selecting the topology with a superior log likelihood value. There were a total of 480 positions in the final dataset. Evolutionary analyses were conducted in MEGA11 (Tamura et al. 2021). The evolutionary history was inferred by using the Maximum Likelihood method and Le_Gascuel_2008 model (Le and Gascuel 2008). The bootstrap consensus tree inferred from 100 replicates (Felsenstein 1985) is taken to represent the evolutionary history of the taxa analyzed. Branches corresponding to partitions reproduced in less than 50% of bootstrap replicates are collapsed. The percentage of replicate trees in which the associated taxa clustered together in the bootstrap test of 100 replicates are shown next to the branches (Felsenstein 1985)

(Trp193 of EcL-RhI, Trp179 of PsL-RhI, Trp187 of LrL-RhI, and Trp137 of SrD-XI), and there are no amino acid residues that could act as an acid/base catalyst to transfer a proton between C1 and C2 through the ene-diol mechanism. This environment enables the catalytic reaction of L-RhIs and D-XIs to adopt a metal-mediated-hydride hydride-shift mechanism (Fig. 1b).

Phylogenetic analysis of L-RhIs and its relationship with that of D-XI

Figure 5 shows the results of phylogenetic analysis of various L-RhIs and D-XI. The initial tree for the heuristic search (Fig. 5a) and the obtained phylogenetic tree after evolutionary analysis (Fig. 5b) are shown. In the initial tree (Fig. 5a), the group is mainly divided into L-RhIs (the upper group) and D-XIs (the lower group) at the beginning. At the next division of the upper group, L-RhIs are divided into a small group including PsL-RhI (PsL-RhI-type) and a large group including EcL-RhI, LrL-RhI, and BhL-RhI (EcL-RhI-type). As the dimer formation of PsL-RhI is similar to that of D-XI, the small group (PsL-RhIs-type) may adopt a D-XI type dimer formation, while the large group of L-RhIs adopts the typical dimer form of EcL-RhI-type. Predicted model structures also support the three categorized types in this phylogenetic tree. In the evolutionary analyzed phylogenetic tree (Fig. 5b) using MEGA11 (Tamura et al. 2021), the group of PsL-RhI-type is evolutionally close to the D-XI- type rather than the EcL-RhI type. Although LrL-RhI is structurally categorized as an EcL-RhI type, it does not have an evolutionally close relationship with EcL-RhI. It may be involved in a specific enzymatic property of LrL-RhI that prefers acidic conditions compared with the optimal pH of EcL-RhI.

Concluding remarks and recent mutagenesis studies

It is known that L-RhI can convert L-lyxose to L-xylulose in *E. coli*. L-lyxose is a rare sugar and cannot be sufficiently catabolized in the next step in wild-type *E. coli*. Although rare sugars are not simply metabolized in bacteria, L-RhIs that exhibit broad substrate specificity can recognize and catabolize some rare sugars. Such enzymes are useful for rare sugar production. In a recent study on aldotetrose production, L-RhI from *P. stutzeri* LL172 was applied to convert D-erythrulose to D-erythrose (Tomino et al. 2023). The substrate recognition of L-RhIs is inherently different from that of D-XIs; however, they share a common $(\beta/\alpha)_8$- barrel fold and a proposed catalytic reaction mechanism based on structural analyses. The flexible loop region is important for enzyme activity and likely related to the evolution based on the analysis of phylogenetic trees between L-RhIs and D-XIs.

Recent studies on protein engineering of some L-RhIs to improve their enzymatic properties have been reported (Chen et al. 2018a, b; Tseng et al. 2022; Duan et al. 2023; Wei et al. 2023). Chen et al. reported a study on the improvement of thermostability and catalytic activity of CaoL-RhI toward D-allulose by site-directed mutagenesis (Chen et al. 2018a, b). In this study, hydrophobic residues located in a predicted β1-α1 loop (flexible loop region) were targeted to be replaced with polar residues by site-directed mutagenesis. Mutant enzymes were designed to decrease the hydrophobic environment and strengthen the catalytic behavior on D-allulose. As a result, the relative activities of the V48N/G59N/I63N and V48N/G59N/I63N/F335S mutants toward D-allulose were increased by 105.6 and 134.1%, respectively, compared with that of the wild-type enzyme. As for the improvement of thermal stability, a mutant enzyme S81A whose hydrophilic residue was replaced with hydrophobic residue was reported. The position of Ser81 is not in the flexible region, but S81A could increase the hydrophobicity through the hydrophobic interaction with Val421 located in the C-terminal α-helix, resulting in enhanced structural stability.

In a report by Tseng et al., the substrate specificity of TsL-RhI was altered by replacing Ile102 with polar or charged residues (Tseng et al. 2022). Ile102 is not located in a predicted flexible loop region, but it is likely located near the flexible region. The catalytic efficiencies of the mutant TsRhIs, I102N, I102Q, and I102R towards D-allose are 148%, 277%, and 191%, respectively, compared with that of the wild-type enzyme, while those toward L-rhamnose are 100%, 167%, and 87%, respectively. In addition, the mutant I102Q showed the highest catalytic efficiency towards D-allose.

Duan et al. reported a study on the improvement of the conversion efficiency of BsL-RhI towards D-allose. In this study, the conversion rate of a mutant D325M and a mutant D325S toward D-allose was increased by 55.73% and by 15.34% at 55 °C, respectively. As the position of Asp325 is predicted at the metal (structural metal) binding site, this position is important. However, the position of D-allulose of the mutants in complex with D-allulose seemed to move in the docking analysis, and the authors speculated that the mutation might affect the affinity between L-RhI and D-allulose (Duan et al. 2023). For these mutants, the structure of the active site may be distorted, making it difficult to predict the metal positions.

Wei et al. demonstrated rational engineering of ClsL-RhI to enhance the stability by computation-aided rational redesign of the flexible regions (Wei et al. 2023). They identified four flexible regions (regions 1 to 4) including the β1-α1 loop region, through molecular dynamics simulations. The identified regions were Region 1 (residues M1-G24), Region 2 (residues V49-D77), Region 3 (residues L226-H247), and Region 4 (residues H364-L388). By truncating the N-terminal α0 α-helix in Region 1, the ΔM1-G24 mutant (M1) demonstrated over 70% higher residual activity compared with that of the wild-type. To further enhance the thermostability of CsL-RI, they conducted rational design mutagenesis against multiple flexible regions (Regions 2, 3, and 4). The resulting combinatorial mutant M2-4 (ΔM1-G24, G57H, G238P, S239Y, L375E) exhibited a 5.7-fold increased half-life at 75 °C and also improved catalytic efficiency.

These protein engineering studies support the improvement of enzyme properties (thermal stability and catalytic efficiency) by altering the flexible regions including the β1-α1 region. Currently, the recombinant L-RhI derived from the probiotic lactic acid bacterium *L. rhamnosus* Probio-M9 is characterized and its structure was also determined (Yoshida et al. 2024). Since the optimum pH of LrL-RhI is pH 5.5, a study on LrL-RhI would provide information for the pH-shift engineering of L-RhI. This pH-shift engineering of L-RhI has not yet been reported, but it may be expected to yield a superior enzyme for rare sugar production.

Acknowledgements The authors are grateful to Prof. Shigehiro Kamitori and our previous colleagues, Dr. Mitsugu Yamada and Dr. Kosei Takeda, for the studies on PsL-RhI. The authors would like to thank Dr. Ian Willey for proofreading this review.

Author contribution HY wrote an original draft. KI and AY reviewed and edited the draft.

Declarations

Ethical approval This article does not include any studies, involving human participants or animals, performed by any of the authors.

Competing interests The authors declare no competing interests.

References

Akhy MT, Brown CM, Old DC (1984) L-Rhamnose utilisation in *Salmonella typhimurium*. J Appl Bacteriol 56:269–274. https://doi.org/10.1111/j.1365-2672.1984.tb01347.x

Al-Zarban S, Heffernan L, Nishitani J, Ransone L, Wilcox G (1984) Positive control of the L-rhamnose genetic system in *Salmonella typhimurium* LT2. J Bacteriol 158:603–608. https://doi.org/10.1128/jb.158.2.603-608.1984

Badia J, Gimenez R, Baldomá L, Barnes E, Fessner WD, Aguilar J (1991) L-lyxose metabolism employs the L-rhamnose pathway in mutant cells of *Escherichia coli* adapted to grow on L-lyxose. J Bacteriol 173:5144–5150. https://doi.org/10.1128/jb.173.16.5144-5150.1991

Bai W, Shen J, Zhu YM, Men Y, Sun YX, Ma YH (2015) Characteristics and kinetic properties of L-rhamnose isomerase from *Bacillus subtilis* by isothermal titration calorimetry for the production of D-allose. Food Sci Technol Res 21:13–22. https://doi.org/10.3136/fstr.21.13

Bhuiyan SH, Itami Y, Izumori K (1997) Isolation of an L-rhamnose isomerase-constitutive mutant of *Pseudomonas* sp. strain LL172: purification and characterization of the enzyme. J Ferment Bioeng 84:319–323. https://doi.org/10.1016/S0922-338X(97)89251-3

Chen Z, Xu W, Zhang W, Zhang T, Jiang B, Mu W (2018a) Characterization of a thermostable recombinant L-rhamnose isomerase from *Caldicellulosiruptor obsidiansis* OB47 and its application for the production of L-fructose and L-rhamnulose. J Sci Food Agric 98:2184–2193. https://doi.org/10.1002/jsfa.8703

Chen Z, Chen J, Zhang W, Zhang T, Guang C, Mu W (2018b) Improving thermostability and catalytic behavior of L-rhamnose isomerase from *Caldicellulosiruptor obsidiansis* OB47 toward D-allulose by site-directed mutagenesis. J Agric Food Chem 66:12017–12024. https://doi.org/10.1021/acs.jafc.8b05107

Domagk GF, Zech R (1963) On the decomposition of desoxy sugars by bacterial enzymes. I. l-Rhamnose-Isomerase from *Lactobacillus plantarum*. Biochem Z 339:145–153

Duan S, Chen Y, Wang G, Li Z, Dong S, Wu Y, Wang Y, Ma C, Wang R (2023) A study of targeted mutation of L-rhamnose isomerase to improve the conversion efficiency of D-allose. Enz Microbial Technol 168:110259. https://doi.org/10.1016/j.enzmictec.2023.110259

Englesberg E (1957) Physiological basis for rhamnose utilization by a mutant of *Pasteurella pestis*. II. A single mutational event leading to the production of two enzymes. Arch Biochem Biophys 71:179–193. https://doi.org/10.1016/0003-9861(57)90020-6

Englesberg E, Baron LS (1959) Mutation to L-rhamnose resistance and transduction to L-rhamnose utilization in *Salmonella typhosa*. J Bacteriol 78:675–686. https://doi.org/10.1128/jb.78.5.675-686.1959

Felsenstein J (1985) Confidence limits on phylogenies: an approach using the bootstrap. Evolution 39:783–791. https://doi.org/10.2307/2408678

Fenn TD, Ringe D, Petsko GA (2004) Xylose isomerase in substrate and inhibitor michaelis states: atomic resolution studies of a metal-mediated hydride shift. Biochemistry 43:6464–6474. https://doi.org/10.1021/bi049812o

Granström TB, Takata G, Tokuda M, Izumori K (2004) Izumoring: a novel and complete strategy for bioproduction of rare sugars. J Biosci Bioeng 97:89–94. https://doi.org/10.1016/S1389-1723(04)70173-5

Hagedoorn PL, Pabst M, Hanefeld U (2024) The metal cofactor: stationary or mobile? Appl Microbiol Biotechnol 108:391. https://doi.org/10.1007/s00253-024-13206-2

Hayashi N, Iida T, Yamada T, Okuma K, Takehara I, Yamamoto T, Yamada K, Tokuda M (2010) Study on the postprandial blood glucose suppression effect of D-psicose in borderline diabetes and the safety of long-term ingestion by normal human subjects. Biosci Biotechnol Biochem 74:510–519. https://doi.org/10.1271/bbb.90707

Iida T, Yamada T, Hayashi N, Okuma K, Izumori K, Ishii R, Matsuo T (2013) Reduction of abdominal fat accumulation in rats by 8-week ingestion of a newly developed sweetener made from high fructose corn syrup. Food Chem 138:781–785. https://doi.org/10.1016/j.foodchem.2012.11.017

Izumori K (2002) Bioproduction strategies for rare hexose sugars. Naturwissenschaften 89:120–124. https://doi.org/10.1007/s00114-002-0297-z

Izumori K (2006) Izumoring: a strategy for bioproduction of all hexoses. J Biotechnol 124:717–722. https://doi.org/10.1016/j.jbiotec.2006.04.016

Jenkins J, Janin J, Rey F, Chiadmi M, van Tilbeurgh H, Lasters I, De Maeyer M, Van Belle D, Wodak SJ, Lauwereys M, Stanssens P, Mrabet NT, Snauwaert J, Matthyssens G, Lambeir A-M (1992) Protein engineering of xylose (glucose) isomerase from *Actinoplanes missouriensis*. 1. Crystallography and site-directed mutagenesis of metal binding sites. Biochemistry 31:5449–5458. https://doi.org/10.1021/bi00139a005

Jiang N, Dillon FM, Silva A, Gomez-Cano L, Grotewold E (2021) Rhamnose in plants - from biosynthesis to diverse functions. Plant Sci 302:110687. https://doi.org/10.1016/j.plantsci.2020.110687

Kim YS, Shin KC, Lim YR, Oh DK (2013) Characterization of a recombinant L-rhamnose isomerase from *Dictyoglomus turgidum* and its application for L-rhamnulose production. Biotechnol Lett 35:259–264. https://doi.org/10.1007/s10529-012-1069-2

Korndörfer IP, Fessner WD, Matthews BW (2000) The structure of rhamnose isomerase from *Escherichia coli* and its relation with xylose isomerase illustrates a change between inter and intra-subunit complementation during evolution. J Mol Biol 300:917–933. https://doi.org/10.1006/jmbi.2000.3896

Kovalevsky AY, Katz AK, Carrell HL, Hanson L, Mustyakimov M, Fisher SZ, Coates L, Schoenborn BP, Bunick GJ, Glusker JP, Langan P (2008) Hydrogen location in stages of an enzyme-catalyzed reaction: time-of-flight neutron structure of D-xylose isomerase with bound D-xylulose. Biochemistry 47:7595–7597. https://doi.org/10.1021/bi8005434

Lavie A, Allen KN, Petsko GA, Ringe D (1994) X-ray crystallographic structures of D-xylose isomerase-substrate complexes position the substrate and provide evidence for metal movement during catalysis. Biochemistry 33:5469–5480. https://doi.org/10.1021/bi00184a016

Le SQ, Gascuel O (2008) An Improved General Amino Acid Replacement Matrix. Mol Biol Evol 25:1307–1320. https://doi.org/10.1093/molbev/msn067

Leang K, Takada G, Ishimura A, Okita M, Izumori K (2004a) Cloning, nucleotide sequence, and overexpression of the L-rhamnose isomerase gene from *Pseudomonas stutzeri* in *Escherichia coli*. Appl Environ Microbiol 70:3298–3304. https://doi.org/10.1128/AEM.70.6.3298-3304.2004

Leang K, Takada G, Fukai Y, Morimoto K, Granstrom TB, Izumori K (2004b) Novel reactions of L-rhamnose isomerase from *Pseudomonas stutzeri* and its relation with D-xylose isomerase via substrate specificity. Biochim Biophys Acta 1674:68–77. https://doi.org/10.1016/j.bbagen.2004.06.003

Levinson SL, Krulwich TA (1976) Metabolism of L-rhamnose in *Arthrobacter pyridinolis*. J Gen Microbiol 96:277–286. https://doi.org/10.1099/00221287-95-2-277

Lin CJ, Tseng WC, Lin TH, Liu SM, Tzou WS, Fang TY (2010) Characterization of a thermophilic L-rhamnose isomerase from *Thermoanaerobacterium saccharolyticum* NTOU1. J Agric Food Chem 58:10431–10436. https://doi.org/10.1021/jf102063q

Lin CJ, Tseng WC, Fang TY (2011) Characterization of a thermophilic L-rhamnose isomerase from *Caldicellulosiruptor saccharolyticus* ATCC 43494. J Agric Food Chem 59:8702–8708. https://doi.org/10.1021/jf201428b

Liu W, Chen M, Duo L, Wang J, Guo S, Sun H, Menghe B, Zhang H (2020) Characterization of potentially probiotic lactic acid bacteria and bifidobacteria isolated from human colostrum. J Dairy Sci 103:4013–4025. https://doi.org/10.3168/jds.2019-17602

Mahmood S, Iqbal MW, Tang X, Zabed HM, Chen Z, Zhang C, Ravikumar Y, Zhao M, Qi X (2024) A comprehensive review of recent advances in the characterization of L-rhamnose isomerase for the biocatalytic production of D-allose from D-allulose. Int J Biol Macromol 254:127859. https://doi.org/10.1016/j.ijbiomac.2023.127859

Moralejo P, Egan SM, Hidalgo E, Aguilar J (1993) Sequencing and characterization of a gene cluster encoding the enzymes for l-rhamnose metabolism in *Escherichia coli*. J Bacteriol 175:5585–5594. https://doi.org/10.1128/jb.175.17.5585-5594.1993

Morimoto K, Suzuki T, Ikeda H, Nozaki C, Goto S (2022) One-pot multi-step transformation of D-allose from D-fructose using a co-immobilized biocatalytic system. J Gen Appl Microbiol 68:1–9. https://doi.org/10.2323/jgam.2021.07.002

Nakamura T, Tanaka S, Hirooka K, Toyoshima T, Kawai N, Tamiya T, Shiraga F, Tokuda M, Keep RF, Itano T, Miyamoto O (2011) Anti-oxidative effects of d-allose, a rare sugar, on ischemia-reperfusion damage following focal cerebral ischemia in rat. Neurosci Lett 487:103–106. https://doi.org/10.1016/j.neulet.2010.10.004

Noguchi C, Kamitori K, Hossain A, Hoshikawa H, Katagi A, Dong Y, Sui L, Tokuda M, Yamaguchi F (2016) d-Allose inhibits cancer cell growth by reducing GLUT1 expression. Tohoku J Exp Med 238:131–141. https://doi.org/10.1620/tjem.238.131

Park CS (2014) Characterization of a recombinant L-rhamnose isomerase from *Bacillus subtilis* and its application on production of L-lyxose and L-mannose. Biotechnol Bioproc Eng 19:18–25. https://doi.org/10.1007/s12257-013-0597-5

Park CS, Yeom SJ, Lim YR, Kim YS, Oh DK (2010) Characterization of a recombinant thermostable L-rhamnose isomerase from *Thermotoga maritima* ATCC 43589 and its application in the production of L-lyxose and L-mannose. Biotechnol Lett 32:1947–1953. https://doi.org/10.1007/s10529-010-0385-7

Poonperm W, Takata G, Okada H, Morimoto K, Granström TB, Izumori K (2007) Cloning, sequencing, overexpression and characterization of L-rhamnose isomerase from *Bacillus pallidus* Y25 for rare sugar production. Appl Microbiol Biotechnol 76:1297–1307. https://doi.org/10.1007/s00253-007-1109-3

Power J (1967) The L-rhamnose genetic system in *Escherichia coli* K-12. Genetics 55:557–568. https://doi.org/10.1093/genetics/55.3.557

Prabhu P, Doan TT, Jeya M, Kang LW, Lee JK (2011) Cloning and characterization of a rhamnose isomerase from *Bacillus halodurans*. Appl Microbiol Biotechnol 89:635–644. https://doi.org/10.1007/s00253-010-2844-4

Prabhu P, Doan TN, Tiwari M, Singh R, Kim SC, Hong MK, Kang YC, Kang LW, Lee JK (2014) Structure-based studies on the metal binding of two-metal-dependent sugar isomerases. FEBS J 281:3446–3459. https://doi.org/10.1111/febs.12872

Ruibo X, Xu L, Weicheng L, Xin S, Heping Z (2023) Reveal the differences in the genome of *Lactobacillus rhamnosus* Probio-M9 and other *Lactobacillus rhamnosus* based on comparative genomics. J Chin Inst Food Sci Technol 23:254–264

Seo MJ, Choi JH, Kang SH, Shin KC, Oh DK (2018) Characterization of L-rhamnose isomerase from *Clostridium stercorarium* and its application to the production of D-allose from D-allulose (D-psicose). Biotechnol Lett 40:325–334. https://doi.org/10.1007/s10529-017-2468-1

Sharma S, Patel SN, Singh SP (2024) A novel thermotolerant L-rhamnose isomerase variant for biocatalytic conversion of D-allulose to D-allose. Appl Microbiol Biotechnol 108:279. https://doi.org/10.1007/s00253-024-13074-w

Shintani H, Shintani T, Sato M (2020) D-Allose, a trace component in human serum, and its pharmaceutical applicability. Int J Appl Biol 11:200–213

Sun Y, Hayakawa S, Puangmanee S, Izumori K (2006) Chemical properties and antioxidative activity of glycated α-lactalbumin with a rare sugar, D-allose, by Maillard reaction. Food Chem 95:509–517. https://doi.org/10.1016/j.foodchem.2005.01.033

Takagi Y, Sawada H (1964) The metabolism of L-rhamnose in *Escherichia coli*. Biochim Biophys Acta 92:10–17. https://doi.org/10.1016/0926-6569(64)90264-0

Takata G, Uechi K, Taniguchi E, Kanbara Y, Yoshihara A, Morimoto K, Izumori K (2011) Characterization of *Mesorhizobium loti* L-rhamnose isomerase and its application to L-talose production. Biosci Biotechnol Biochem 75:1006–1009. https://doi.org/10.1271/bbb.110018

Tamura K, Stecher G, Kumar S (2021) MEGA11: molecular evolutionary genetics analysis version 11. Mol Biol Evol 38:3022–3027. https://doi.org/10.1093/molbev/msab120

Tomino S, Yoshihara A, Fleet GWJ, Izumori K (2023) Production of d-aldotetrose from l-erythrulose using various isomerases. Biosci Biotechnol Biochem 87:850–856. https://doi.org/10.1093/bbb/zbad058

Tseng WC, Chen YC, Chang HC, Lin CJ, Fang TY (2022) Altering the substrate specificity of recombinant L-rhamnose isomerase from *Thermoanaerobacterium saccharolyticum* NTOU1 to favour D-allose production. J Biotechnol 358:9–16. https://doi.org/10.1016/j.jbiotec.2022.08.015

Wei M, Gao X, Zhang W, Li C, Lu F, Guan L, Liu W, Wang J, Wang F, Qin HM (2023) Enhanced thermostability of an L-rhamnose isomerase for d-allose synthesis by computation-based rational redesign of flexible regions. J Agric Food Chem 71:15713–15722. https://doi.org/10.1021/acs.jafc.3c05736

Whitlow M, Howard AJ, Finzel BC, Poulos TL, Winborne E, Gilliland GL (1991) A metal-mediated hydride shift mechanism for xylose isomerase based on the 1.6 A *Streptomyces rubiginosus* structures with xylitol and D-xylose. Proteins 9:153–173. https://doi.org/10.1002/prot.340090302

Wilson DM, Ajl S (1957) Metabolism of l-rhamnose by *Escherichia coli* I Lrhamnose Isomerase. J Bacteriol 73:410–414. https://doi.org/10.1128/jb.73.3.410-414.1957

Xu W, Zhang W, Tian Y, Zhang T, Jiang B, Mu W (2017) Characterization of a novel thermostable l-rhamnose isomerase from *Thermobacillus composti* KWC4 and its application for production of d-allose. Process Biochem 53:153–161. https://doi.org/10.1016/j.procbio.2016.11.025

Yoshida H, Yamada M, Ohyama Y, Takada G, Izumori K, Kamitori S (2007) The structures of l-rhamnose isomerase from *Pseudomonas stutzeri* in complexes with l-rhamnose and d-allose provide insights into broad substrate specificity. J Mol Biol 365:1505–1516. https://doi.org/10.1016/j.jmb.2006.11.004

Yoshida H, Takeda K, Izumori K, Kamitori S (2010a) Elucidation of the role of Ser329 and the C-terminal region in the catalytic activity of *Pseudomonas stutzeri* l-rhamnose isomerase. Protein Eng Des Sel 23:919–927. https://doi.org/10.1093/protein/gzq077

Yoshida H, Yamaji M, Ishii T, Izumori K, Kamitori S (2010b) Catalytic reaction mechanism of *Pseudomonas stutzeri* l-rhamnose isomerase deduced from X-ray structures. FEBS J 277:1045–1057. https://doi.org/10.1111/j.1742-4658.2009.07548.x

Yoshida H, Yoshihara A, Teraoka M, Yamashita S, Izumori K, Kamitori S (2012) Structure of l-rhamnose isomerase in complex with l-rhamnopyranose demonstrates the sugar-ring opening mechanism and the role of a substrate sub-binding site. FEBS Open Bio 3:35–40. https://doi.org/10.1016/j.fob.2012.11.008

Yoshida H, Yamamoto N, Kurahara LH, Izumori K, Yoshihara A (2024) X-ray structure and characterization of a probiotic *Lactobacillus rhamnosus* Probio-M9 L-rhamnose isomerase. Appl Microbiol Biotechnol 108:249. https://doi.org/10.1007/s00253-024-13075-9